Spectrum of Engineering Sciences
ISSN (e) 3007-3138 (p) 3007-312X Volume 4, Issue 1, 2026

NUMERICAL SIMULATION AND PERFORMANCE OPTIMIZATION OF A LEAD-FREE Rb_2SnBr_6-BASED PEROVSKITE SOLAR CELL USING SCAPS-1D

Qosia Laraib[1], Shanza Ali[2], Ahmed Salim[3], Mohsin M. Tarar[4], Azmat Ali[*5]

[1,2,*5]*Department of Physics, University of Chakwal, Chakwal, Pakistan*
[3]*Department of Electrical Engineering, NAMAL University Mianwali, Pakistan*
[4]*Department of Electronics Engineering, University of Chakwal, Chakwal, Pakistan*

[1]qosialaraib@gmail.com, [2]shanzaali904@gmail.com, [3]ahmed.salim@namal.edu.pk, [4]mohsin.tarar@uoc.edu.pk, [*5]azmat.chakwal@gmail.com

DOI: http://doi.org/10.5281/zenodo.18995554

Keywords
Perovskites, Solar Energy, lead Free, SCAPS-1D, Numerical Simulations

Article History
Received: 22 November 2025
Accepted: 15 January 2026
Published: 30 January 2026

Corresponding Author: *
Azmat Ali

Abstract

This study reports a numerical investigation of a lead-free perovskite solar cell towards addressing the limitations of toxicity and stability imposed on conventional lead based solar cells. A v
acancy-ordered double perovskite, Rb_2SnBr_6, was used as the absorber layer and examined by the SCAPS-1D simulation tool. The proposed device structure is FTO/TiO_2/Rb_2SnBr_6/CuI/Au where TiO_2 and CuI serve as an electron and hole transport layer, respectively. Key device parameters such as absorber thickness, defect density, ETL thickness, donor density and work temperatures have been systematically optimized in order to improve the photovoltaic device performance. Using the optimized conditions, the power conversion efficiency of the device was found to be 32.66%, an open circuit voltage of 1.154 V, a short circuit current density of 31.64 mA/cm^2, and a fill factor of 89.44%. These results demonstrate the high potential of Rb_2SnBr_6 as a stable and non-toxic absorber material for high efficiency lead-free perovskite solar cells.

INTRODUCTION

The ever-growing global electricity demand is caused by both the rapidly growing industry and business and technological progress[1]. Currently, fossil fuels (coal, natural gas, petroleum) are used to satisfy the majority of electricity demand[2]. However, the continued use of these forms of non-renewable energy will present serious problems with respect to global warming and other types of environmental pollution[3]. Consequently, developing new forms of renewable energy technologies will be one of science and technology's greatest challenges and will be expensive to implement[4]. Among several sustainable power alternatives (wind, hydro, tidal, geothermal, and bioenergy)[5], solar energy has been regarded as the most beneficial due to its abundance, accessible nature, and low environmental impact[6]. The rapid
increase in cell efficiencies, combined with the decreasing cost of solar panel technology has led to a viable means of reducing dependence on fossil fuels [4, 7]. However, in order for solar power to compete with conventional energy systems, continued improvements are required for power conversion efficiency (PCE), long-term stability, and manufacturing costs[8]. The ultimate source of these advances will be based on the finding of the new absorbers or the new types of solar cells that are efficient, stable, and environmental friendly.

At that, halide perovskite materials have become one of the most remarkable ones with the great optoelectronic characteristics, tunable bandgap, large absorption coefficient, and solubility in solutions[9, 10].

The first generation of lead-halide-based perovskite solar cells was proven to perform excellently and attain power conversion efficiencies of more than 25%[11]. Although successful, lead-based perovskites have inherent toxicity and low chemical stability, making it difficult at a large scale commercialization and very serious in environmental issues[12]. All of these disadvantages have prompted researchers to consider lead-free alternatives that are safer and more stable but would allow preserving the high level of performance of the devices[13].

Among the most promising paths that this search is taking is the development of vacancy-ordered double perovskites (A_2BX_6), with A-site is a monovalent cation (Cs^+, Rb^+ or K^+), B-site is a tetravalent metal cation (Sn^{4+}, Ti^{4+} or Zr^{4+}), and X being a halide anion (I^-, Br^- or Cl^-,)[14]. The materials are chemically highly tunable, highly moisture resistant, inherently lead-free and high structural stable, which is why they are good candidates of next-generation photovoltaic and optoelectronic applications [14, 15]. One of these compounds, Rb_2SnBr_6 (rubidium tin(IV) bromide) has stood out as a promising, stable, and non-toxic semiconductor in this group with promising optical and electronic properties applicable in solar cell applications and other optoelectronic applications[16, 17]. In this article, numerical simulation of a lead-free perovskite solar was analyzed with Rb_2SnBr_6 as a absorber using SCAPS-1D software[18]. The structure of device is **FTO/TiO_2/Rb_2SnBr_6/CuI/Au**. Under this

design, TiO_2 is used as ETL in which it assists in gathering high-energy electrons at the absorber and reducing unwanted charge recombination at the interface[19]. Conversely, CuI is used as the layer of hole transport (HTL), which directs the lower energy holes to the back contact[20]. With these layers fixed, we examined the effect of a variety of factors on overall device efficiency. We analyzed the variation in the performance of solar cell by changing absorber thickness, its defect density, ETL thickness, donor density of ETL, and operating temperature. The main objective of this study to discover the appropriate layer sizes and material characteristics that could enhance the power conversion efficiency (PCE) also makes the device easy and affordable. The findings of the present work can be fruitfully used to develop stable, non-toxic, and ecologically friendly perovskite solar cells that will be able to work under various conditions.

Methodology

SCAPS-1D (Solar Cell Capacitance Simulator), a one-dimensional simulation program developed at the University of Gent[21] was employed to conduct the numerical analysis of the proposed lead-free perovskite solar cell[22]. This software finds a wide usage in investigating the thin-film photovoltaic devices because it can predict the behavior of the devices in varying operation conditions. The photovoltaic parameters that are important like V_{oc}, J_{sc}, FF, PCE, and quantum efficiency can be calculated using SCAPS-1D [22-24].

The equations used to simulate the device structure are the self-consistent Poisson, electron continuity equation and holes continuity equation, which are all fundamental equations of semiconductor[25].

Poisson's equation is

$$\frac{d}{dx}\left(-\varepsilon(x)\frac{d\psi}{dx}\right) = q[\,p(x) - n(x) + N_D^+(x) - N_A^-(x) + p_t(x) - n_t(x)\,] \quad (1)$$

Ψ is electrostatic potential, p and n are respective hole and electron ε is relative permittivity. N_A Acceptor density and N_d is donor density [25, 26]

The carrier continuity equation is represented as

$$-\frac{\partial j_p}{\partial x} + G - U_p(n,p) = 0 \quad (2)$$

$$-\frac{\partial j_n}{\partial x} + G - U_n(n,p) = 0 \quad (3)$$

J_p and J_n hole and electron current density, G is carrier generation rate, $U_p(n,p)$ and $U_n(n,p)$ are the hole and electron recombination rates respectively[27].

Carrier current density

$$j_p = qnU_pE - qD_p\frac{\partial p}{\partial x} \quad (4)$$

$$j_n = qnU_nE - qD_n\frac{\partial n}{\partial x} \quad (5)$$

D_p and D_n are diffusion coefficient and U_p and U_n are carrier mobility [28].

The structure used to simulate solar cell is FTO/TiO_2/Rb_2SnBr_6/CuI/Au. The structure of the schematic device and the alignment of the energy bands are presented in

Figure 1(a) and

Figure 1(b), respectively. The reported literature and experimentally confirmed studies provided material parameters of band gap, electron affinity, dielectric constant, carrier mobility, density of defects and effective density of states of each layer **[29-32]**. Error! Reference source not found. **show these parameters that we employed in SCAPS-1D.** Systematical variation of absorber layer thickness was carried out to study its influence on the performance of the device and, ETL was optimized to reduce recombination and series resistance losses[28].
The AM 1.5G illumination with a power density of 1000 W/m^2 was used for simulation, which is typical test conditions. It was first adjusted to 300 K operating temperature which was then monitored to assess thermal stability [23]

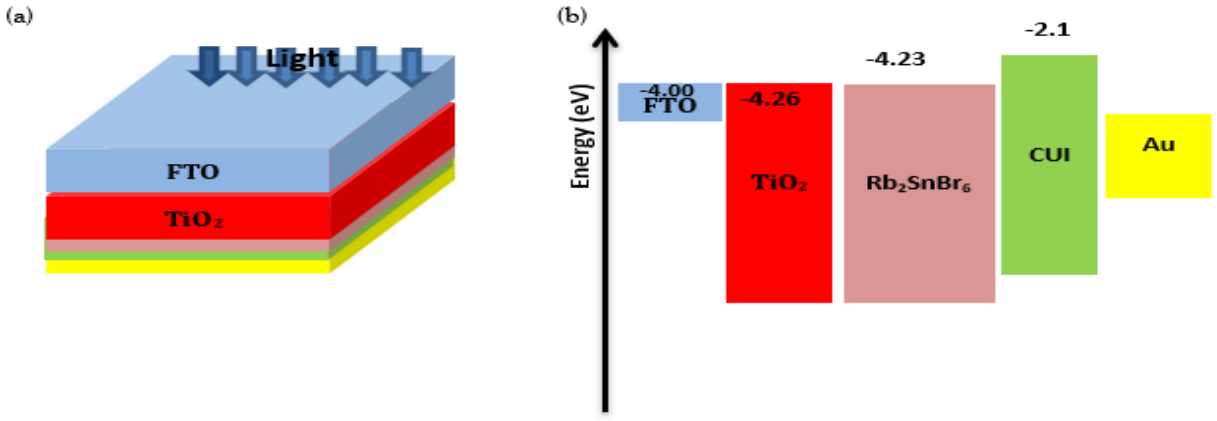

Figure 1 (a) Schematics diagram of simulated PSC , (b) Energy band diagram of PSCs

Table 1. Input parameters used in the simulation

Parameters	FTO [29]	TiO_2 [30]	CuI [31]	Rb_2Snbr_6 [32]
Thickness (nm)	50	50	200	850
E_g (eV)	3.6	3.26	3.1	1.4
χ (eV)	4	4.26	2.1	4.23
ε_r	9	32	6.5	16.70
N_c ($1/cm^3$)	2.2×10^{18}	1.0×10^{19}	2.8×10^{19}	1.0×10^{18}
N_v ($1/cm^3$)	1.8×10^{19}	1.0×10^{19}	1.0×10^{19}	1.0×10^{21}
μ_n ($cm^2/V.s$)	100	20	100	42
μ_p ($cm^2/V.s$)	25	10	43.9	310
N_D ($1/cm^3$)	1.0×10^{18}	1.0×10^{17}	0	0
N_A ($1/cm^3$)	0	0	1.0×10^{18}	1.0×10^{20}
N_t ($1/cm^3$)	1.0×10^{14}	1.0×10^{15}	1.0×10^{15}	1.0×10^{13}

Table 2.The values of defect density within the layers and interface of the device [30-32]

Parameters	ETL	HTL	Rb_2SnBr_6	HTL/Rb_2SnBr_6	Rb_2SnBr_6/ETL
Defect Type	Neutral	-	-	-	-
Capture cross section For σ_n, σ_p (cm^{-2})	1.0×10^{-15}	1.0×10^{-15}	1.0×10^{-15}	1.0×10^{-19}	1.0×10^{-19}
Energetic distribution	Single	Single	Single	Single	Single
Energy level with respect to E_v (eV)	0.6	0.6	0.6	0.6	0.6
Characteristic energy(eV)	0.1	0.1	0.1	0.1	0.1
N_t (cm^{-3})	1×10^{15}	1×10^{15}	1×10^{13}	1×10^{10}	1×10^{10}

Effect of absorber thickness

The absorbing layer thickness is an important structural parameter that has a great impact on the overall perovskite solar cell performance. In order to study this effect, the absorber of Rb_2SnBr_6 was made with a range of 100-2000 nm with all other parameters of the device held constant as presented in **Error! Reference source not found.**. The parameters of the devices (V_{OC}, J_{SC}, FF, and PCE) grow quickly until about 1000 nm

absorber thickness, and then the growth is slow, showing a saturation curve **Figure 2**. The increase in performance up to 1000nm is primarily attributed to the increased photon absorption and the density of photogenerated carriers in the absorber[18]. More than this thickness, the further enhancement is of no value since the substance has already swept up the majority of the incident photons, and then no more carriers are produced significantly. So, the most appropriate absorber thickness in this paper was identified as 1000 nm and it was chosen to be used in additional simulation of the device.

With an optimal thickness, Rb_2SnBr_6-based perovskite solar cell achieved a V_{oc} of 1.1530 V, a J_{sc} of 31.63mA/cm^2, and a FF of 89.42%, a PCE of 32.61% indicating that the ideal combination of carrier extraction and light absorption was at 1000 nm.

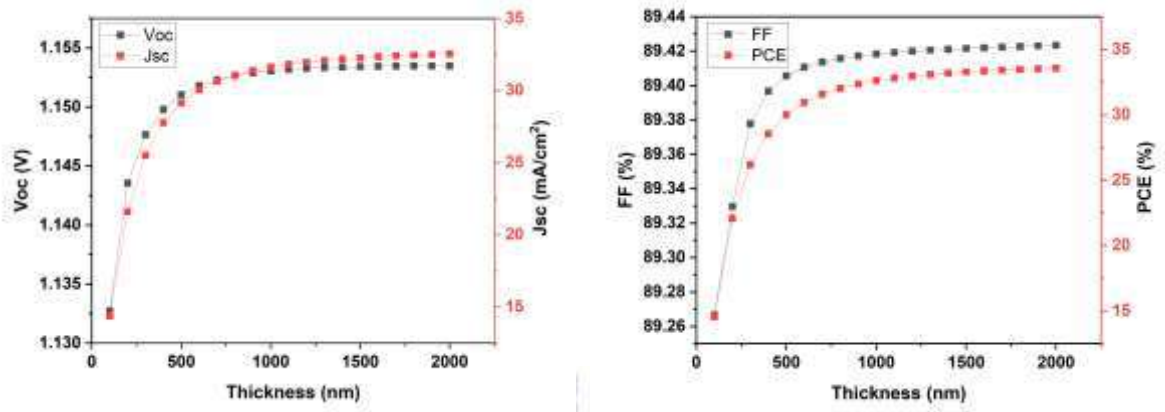

Figure 2. Effect of absorber layer thickness on PSC device

Effect of absorber Defect density

The stability of photovoltaic devices depends on the defect density of the absorber layer that also plays a great role in the overall effectiveness of the device. To make the photovoltaic (PV) output parameters constant, it is importance to control the quantity of the defects in the absorber layer. Generation and recombination of electron-hole pairs are directly affected by defect density, which has an impact on the perovskite solar cells (PSCs) efficiency [33, 34]. Defect density is largely dependent on the quality of structure of absorber layer; low material quality leads to increase in the quantity of defects. Subsequently, more defect
density is associated with higher charge carrier recombination that eventually leads to the decrease in device efficiency[35].

The reason why the diffusion length of charge carriers is closely related to the recombination rate is that the bulk defect density of the PSC also dictates the diffusion length of charge carriers. Shockley-Read-Hall (SRH)-recombination-mechanism dominates the perovskite solar cells[23].The trap-assisted SRH recombination model can thus be used to assess the diffusion length. The SRH recombination rate is expressed by Equations **(6)** and **(7)[36]**

$$\mathbf{R_{SRH}} = \frac{\mathbf{np - n_{i^2}}}{\left[\boldsymbol{\pi}\left(\mathbf{p+n+\frac{2n_i \cosh(E_i - E_t)}{kT}}\right)\right]} \quad (8)$$

$$\boldsymbol{\tau} = \frac{\mathbf{1}}{[\boldsymbol{\sigma} \times \mathbf{N_t} \times \mathbf{V_{th}}]} \quad (9)$$

Where, τ denotes the charge carrier lifetime, σ represents the capture cross-section, (N_t) is perovskite absorber film defect density, and (V_{th}) is charge carriers thermal velocity. The diffusion length $L = \sqrt{D\tau}$ where D refers the diffusion coefficient [37].
The dependence of the V_{oc} on defect density is described by Equation **(10)**

$$V_{oc} = \frac{kT}{q} \ln\left(\frac{J_{sc}}{J_o} + 1\right) \qquad (11)$$

The best defect density was determined by the performance of the PSCs where the absorber layer defect density was varied to a maximum of 10^{12}cm^{-3} to 10^{17} cm^{-3}.**Figure 3** demonstrates that the photovoltaic parameters are all on the decline with the rise in the defect density. The V_{oc} decreases from 1.15 to 1.01 V and the J_{sc} decreases from 31.6 to 20.6 mA/cm^2 showing that the recombination increases significantly at elevated N_t. The FF drops marginally, 89.4% to 88.2% and the PCE drops drastically from 32.7% to 18.6%. The PCE and FF almost does not vary in the low-defect region (10^{12}-10^{14} cm^{-3}) but at a higher level PCE and FF decrease beyond 10^{15} cm^{-3} owing to high recombination. J-V characteristics for different defect densities are given in **Figure 4**. According to the results, the optimum defect density that maximizes efficiency of the device was found to be 10^{12} cm^{-3}. This is the optimal value of the device, and it has been demonstrated that to ensure efficient operation of the perovskite solar cell, the number of trap states in the Rb_2SnBr_6 layer must be minimized.

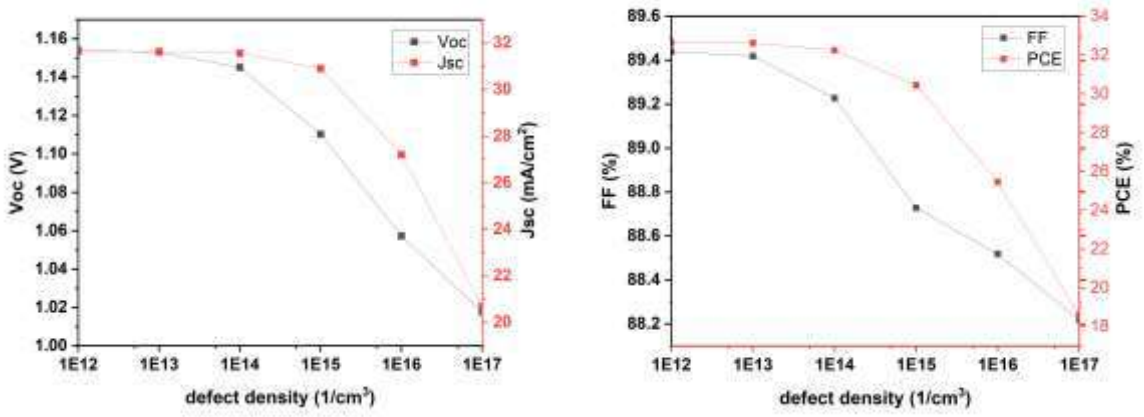

Figure 3. Dependence of absorber layer defect density on V_{oc}, J_{sc}, FF, PCE

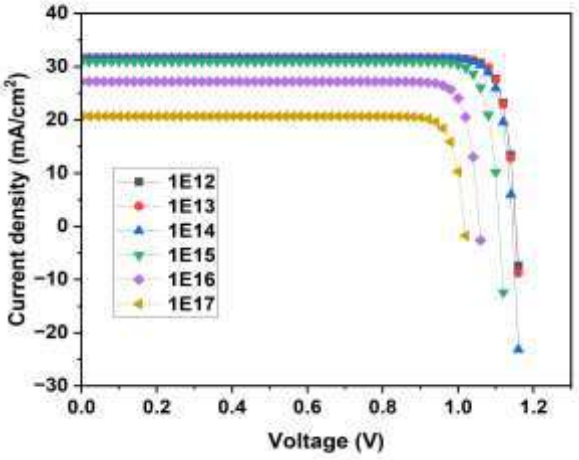

Figure 4. Comparison of J-V curves for different defect density.

Effect of ETL thickness

One important factor in the perovskite solar cells is the electron transport layer (ETL) thickness which determines the charge extraction and hole blocking, and interfacial recombination inhibition[38]. To determine this effect, the thickness of the ETL was varied within a range of 20-200 nm, and all the other parameters of the devices were kept the same. As Per **Figure 5**, the simulated data reveal that as the ETL thickness increases, there is a small yet steady increase in V_{oc} which can be explained by interfacial recombination essentially being decreased and the electrostatic field at the interface between the ETL and the absorber being stabilized. The J_{sc} however decreases with increasing thickness. The main cause of this decrease is the longer pathway of transport and the increased series resistance in the thicker ETLs that prevent easy extraction of electrons[39]. At moderate thickness values, there are also witnessed a slight increase in fill factor (FF) that can probably be attributed to the low leakage and increased carrier selectivity. Despite this, the total PCE reduces continuously above a given thickness as the loss of Jsc predominates over the minor increases of Voc and FF. The device is most effectively manifested under ETL thickness of 50 nm, which yields a V_{oc} of 1.15 V, J_{sc} of 31.6mA/cm^2, FF of 89.4% and PCE of 32.7%. Thus a thickness of 50 nm is decided as optimum thickness of ETL to enhance maximum efficiency of device in such structure.

Effect of ETL Donor density

The donor concentration of the electron transport layer (ETL) is one of the most critical parameters that affect the charge transportation and electrification formation and recombination processes in perovskite solar cells. The donor density of ETL was changed in the range of 10^{14} to 10^{20} cm^{-3} but the parameters of other devices remained constant in order to analyze its influence[37].

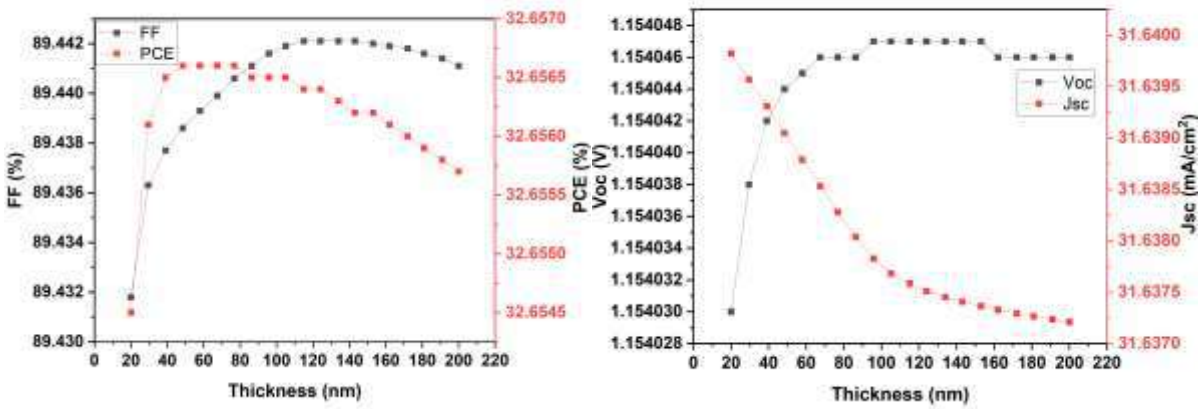

Figure 5. Effect of ETL thickness on Voc, Jsc, FF, PCE

The corresponding variations in the photovoltaic parameters are presented in **Figure 6**. As observed from the result V_{oc} will be almost the same at the donor density of 10^{14} to 10^{17} cm^{-3} suggests that the junction formation and the charge extraction is stable and efficient in this density. A marginal decrease in Voc is noticed beyond $10^{17}cm^{-3}$ which become more evident at $10^{20}cm^{-3}$. This behavior is explained by the fact that it increases carrier recombination losses at high levels of doping [40].

Similarly, short-circuit current density (J_{sc}) showed a constant tendency until a donor concentration of $10^{17}cm^{-3}$ which indicates that generation and collection of carriers is not significantly influenced at moderate levels of doping. After this value, there is a gradual loss in J_{sc} which can be attributed to an enhancement of the impurity scattering and slower carrier movement in the ETL at higher donor densities. The fill factor (FF) and PCE both show the constant value at the range of 10^{14} to 10^{17} cm^{-3} after that there is slight decline at the $10^{19}cm^{-3}$ and then there is also slight increment in the FF and PCE[41].

These observations are further supported by the J-V characteristics in **Figure 7** which show that the curves of donor densities coincide with each other showing a stable operation of the devices. Thus, a donor density of 10^{15} cm^{-3} is chosen as it is the most balanced and stable device performance and excessive doping has an adverse influence on the charge transport and the total efficiency.

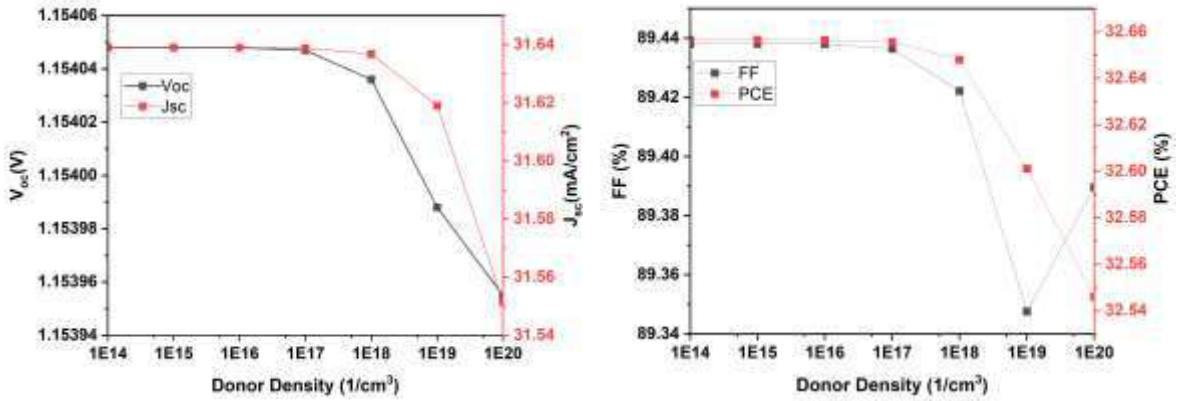

Figure 6. Effect of Donor density of ETL (TiO_2) on Voc, Jsc, FF, PCE

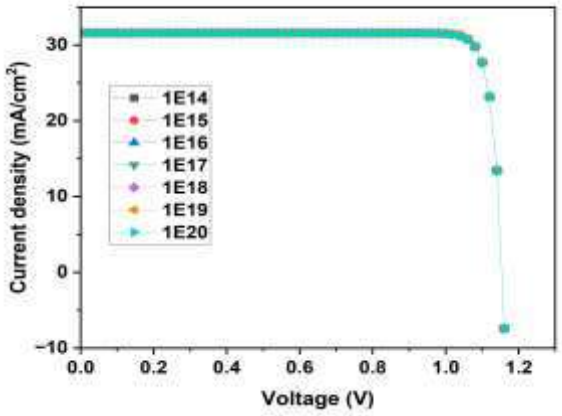

Figure 7. Comparison of J-V curves for different donor density.

Effect of Temperature

The operating temperature has a relatively less or more influence on the photovoltaic behavior of the perovskite solar cells, especially in the conditions that occur under the sun where the solar cells are continuously exposed to thermal conditions [40]. To examine this effect, the performance of the device was examined within the temperature range of 250-500 K, and the change in the primary photovoltaic parameters was plotted in **Figure 8.**

At 250K to 300K, there is a sharp rise in the short-circuit current density (J_{sc}) because carrier transport is enhanced and trapping is also minimized. At temperatures above 300 K, J_{sc} adopts an almost saturated behavior with very slight extreme variation meaning that increase in temperature does not provide significant increase in current generation due to competing recombination mechanisms. In contrast, Open-circuit voltage (V_{oc}) declines continuously with temperature, primarily because of the decreased band-gap and increased defect-assisted recombination[42]. Also, the fill factor (FF) is constantly reducing, and this shows an increase of resistive losses at high temperatures. The PCE rises and attains a peak value of 300 K. Nevertheless, PCE slowly decreases at temperature over 300 K, despite the fact that J_{sc} changes slightly[43]. This behavior is also verified by the J-V characteristics in **Figure 9** which exhibit low voltage output and poor curve shape at high temperatures. Comprehensively, the findings show that 300 K has been the best operating temperature of the device although temperatures above it cause losses in efficiency primarily because of voltage and fill factor losses.

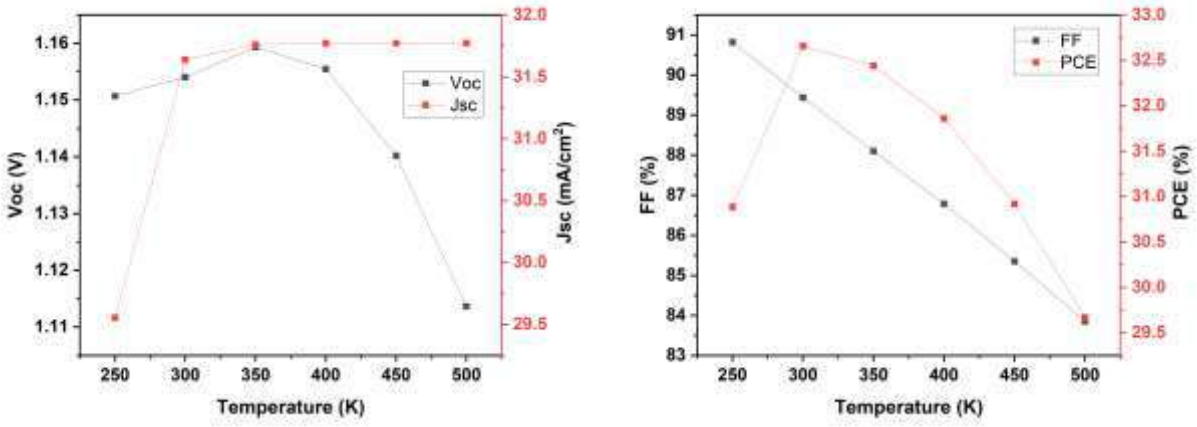

Figure 8. Variation of Voc, Jsc, FF, PCE with respect to Temperature.

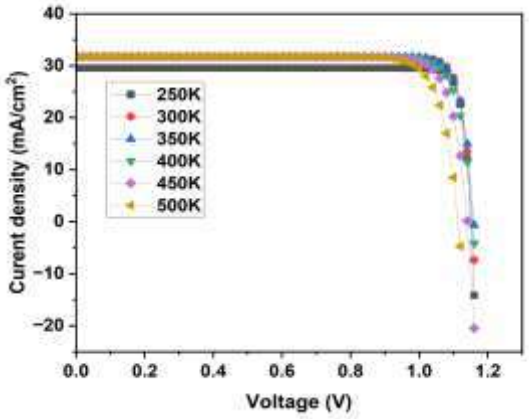

Figure 9. J-V curve with varied temperature

Performance of energy band diagram

Cliff and spike geometry at the electron transport layer (ETL)/absorber interface is a major determinant of performance of a solar cell. The effects of these Band Offsets are on charge transport and recombination. An offset in the negative conduction band (CBO) that is referred to as a cliff structure, enables electron back-transfer that can lead to an increase in interfacial recombination. Conversely, a small positive CBO creates a spike-like barrier which inhibits recombination yet enhances effective extraction of electrons, hence the enhancement of the efficiency of the device [44]. The band diagrams of the solar cell structures are given in Fig. 10

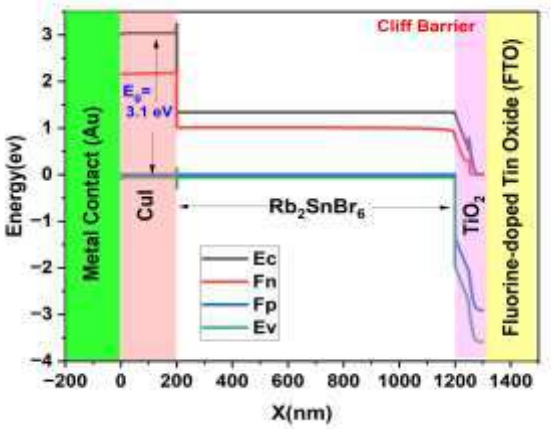

Figure 10. Energy band diagram of optimized solar cell

Performance of optimized device

Fig.11 indicates J-V characteristic curve of optimized solar cell using FTO/TiO_2/Rb_2SnBr_6/CuI/Au cell structure. In the optimized structure, the donor density of the electron transport layer (TiO_2) is set to 10^{15} cm^{-3}. The absorber layer thickness is optimized to 1000 nm, and its defect density is fixed at 10^{12} cm^{-3} to suppress non-radiative recombination. Under these optimized conditions, the device has V_{oc} of **1.1540 V**, J_{sc} **of 31.64** mA/cm^2, a fill factor (FF) of **89.44** %, and a high power conversion efficiency (PCE) of **32.66 %.**

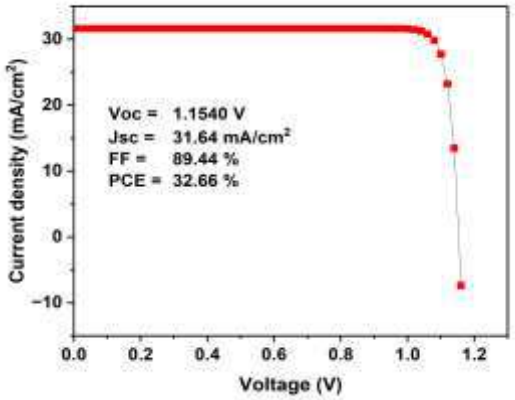

Figure 11. J-V characteristic curve for optimized device with FTO/TiO2/Rb_2SnBr_6/CUI/Au structure

Conclusion

In conclusion, a lead-free perovskite solar cell using Rb_2SnBr_6 as an absorber layer was numerically studied and optimized using the numerical SCAPS-1D simulator. Key device parameters such as absorber and ETL thickness, defect density, donor density and operating temperature were systematically analyzed to improve the photovoltaic performance. Through careful optimization, the power conversion efficiency of the device reached **32.66%**. These findings confirm the fact that the material properties and the arrangement of the layers that are used have to be strictly controlled to achieve the optimal performance of lead-free perovskite solar cells.

Overall, this study holds great promise for the potential of Rb_2SnBr_6 as a stable, environmental friendly absorber material, and it also gives useful guidance for the design and creation of efficient sustainable Perovskite photovoltaic devices.

References

1. Mir, A.A., et al., *A review of electricity demand forecasting in low and middle income countries: The demand determinants and horizons.* Sustainability, 2020. **12**(15): p. 5931.https://doi.org/10.3390/su12155931
2. Thompson, S., *Strategic analysis of the renewable electricity transition: power to the world without carbon emissions?* Energies, 2023. **16**(17): p. 6183.https://doi.org/10.3390/en16176183
3. Wolf, S., et al., *Scientists' warning on fossil fuels.* Oxford Open Climate Change, 2025. **5**(1): p. kgaf011.https://doi.org/10.1093/oxfclm/kgaf011
4. Eti, S., et al., *Assessment of technical and financial challenges for renewable energy project alternatives.* Cleaner Engineering and Technology, 2024. **18**: p. 100719.https://doi.org/10.1016/j.clet.2023.100719
5. Sayed, E.T., et al., *A critical review on environmental impacts of renewable energy systems and mitigation strategies: Wind, hydro, biomass and geothermal.* Science of the total environment, 2021. **766**: p. 144505.https://doi.org/10.1016/j.scitotenv.2020.144505
6. Maka, A.O. and J.M. Alabid, *Solar energy technology and its roles in sustainable development.* Clean Energy, 2022. **6**(3): p. 476-483.https://doi.org/10.1093/ce/zkac023
7. Ugochukwu, A.A., et al., *Recent enhancement in photovoltaic cell efficiency performance, stability, and cost reduction: a review.* Solar Energy, 2025. **300**: p. 113853.https://doi.org/10.1016/j.solener.2025.113853
8. Al-Ali, S., A.G. Olabi, and M. Mahmoud, *A review of solar photovoltaic technologies: developments, challenges, and future perspectives.* Energy Conversion and Management: X, 2025: p. 101057.https://doi.org/10.1016/j.ecmx.2025.101057

9. Polavarapu, L., et al., *Introduction to halide perovskite optoelectronics.* Nanoscale, 2023. **15**(37): p. 15075-15078.https://doi.org/10.1039/D3NR90170J
10. Sheng, M., et al., *Accelerated discovery of halide perovskite materials via computational methods: a review.* Nanomaterials, 2024. **14**(13): p. 1167.https://doi.org/10.3390/nano14131167
11. Fan, X., *Advanced progress in metal halide perovskite solar cells: A review.* Materials Today Sustainability, 2023. **24**: p. 100603.https://doi.org/10.1016/j.mtsust.2023.100603
12. Ahmed, I., K. Prakash, and S.M. Mobin, *Lead-free perovskites for solar cells applications: recent progress, ongoing challenges, and strategic approaches.* Chemical Communications, 2025.https://doi.org/10.1039/D4CC06835A
13. Miah, M.H., et al., *Lead-free alternatives and toxicity mitigation strategies for sustainable perovskite solar cells: a critical review.* Materials Advances, 2025. **6**(9): p. 2718-2752.https://doi.org/10.1039/D5MA00010F
14. Faizan, M., et al., *Electronic and optical properties of vacancy ordered double perovskites A2BX6 (A= Rb, Cs; B= Sn, Pd, Pt; and X= Cl, Br, I): a first principles study.* Scientific reports, 2021. **11**(1): p. 6965.https://doi.org/10.1038/s41598-021-86145-x
15. Chu, L., et al., *Lead-free halide double perovskite materials: a new superstar toward green and stable optoelectronic applications.* Nano-Micro Letters, 2019. **11**(1): p. 16.https://doi.org/10.1007/s40820-019-0244-6
16. Hasan, R., et al., *Hydrothermal growth and characterization of large Rb 2 SnBr 6 double perovskite crystals: a promising semiconductor material for photocatalysis and optoelectronics.* Dalton Transactions, 2025. **54**(9): p. 3796-3803.https://doi.org/10.1039/D4DT02712D
17. Apon, I.A., et al., *Rb 2 BX 6 double perovskites: unlocking 22% efficiency through structural, electronic, mechanical, and optical insights.* RSC advances, 2025. **15**(47): p. 40209-40230.https://doi.org/10.1039/D5RA03981A
18. Reza, M.S., et al., *Simulation and machine learning driven optimization of RB 2 SNBR 6-Based Lead-Free perovskite solar cells using diverse ETLs for enhanced photovoltaic performance.* Materials Advances, 2025. **6**(24): p. 9602-9626.https://doi.org/10.1039/D5MA00955C
19. Zhao, W., et al., *TiO2 electron transport layer with p–n homojunctions for efficient and stable perovskite solar cells.* Nano-Micro Letters, 2024. **16**(1): p. 191.https://doi.org/10.1007/s40820-024-01407-3
20. Pau, R., et al., *Solution-processed CuI as a hole transport layer for Sn–Pb perovskite solar cells.* Journal of Materials Chemistry A, 2025. **13**(48): p. 42118-42127.https://doi.org/10.1039/D5TA06770G
21. Khatoon, S., et al., *Design of a CH3NH3PbI3/CsPbI3-based bilayer solar cell using device simulation.* Heliyon, 2022. **8**(7).https://doi.org/10.1016/j.heliyon.2022.e09941
22. Meyer, E.L., et al., *Computational study of chalcogenide-based perovskite solar cell using SCAPS-1D numerical simulator.* Materials, 2025. **18**(1): p. 186.https://doi.org/10.3390/ma18010186
23. Abdullah, M.I., et al., *Numerical modeling and performance optimization of all inorganic Pb free novel NaSnCl3 based perovskite solar cells via SCAPS-1D framework.* Scientific Reports, 2025. **15**(1): p. 41709.https://doi.org/10.1038/s41598-025-25714-w
24. Araújo, V.H.D., et al., *Advances in lead-free perovskite solar cell design via SCAPS-1D simulations.* RSC Sustainability, 2025. **3**(10): p. 4314-4335.https://doi.org/10.1039/D5SU00526D
25. Raoui, Y., et al., *Performance analysis of MAPbI3 based perovskite solar cells employing diverse charge selective contacts: Simulation study.* Solar Energy, 2019. **193**: p. 948-955.https://doi.org/10.1016/j.solener.2019.10.009
26. Rahman, M.B., et al., *Selection of a compatible electron transport layer and hole transport layer for the mixed perovskite FA 0.85 Cs 0.15 Pb (I 0.85 Br 0.15) 3, towards achieving novel structure and high-efficiency perovskite solar cells: a detailed numerical study by SCAPS-1D.* RSC advances, 2023. **13**(25): p. 17130-17142.https://doi.org/10.1039/D3RA02170J

27. Ahmad, O., et al., *Performance evaluation of Au/p-CdTe/Cs2TiI6/n-TiO2/ITO solar cell using SCAPS-1D.* Optical Materials, 2021. **117**: p. 111105.https://doi.org/10.1016/j.optmat.2021.111105
28. Utsho, K.I.F., et al., *Optimizing Cs 2 CuBiBr 6 double halide perovskite for solar applications: the role of electron transport layers in SCAPS-1D simulations.* RSC advances, 2025. **15**(3): p. 2184-2204.https://doi.org/10.1039/D4RA08515A
29. Hosen, A. and S.R. Al Ahmed, *Performance analysis of SnS solar cell with a hole transport layer based on experimentally extracted device parameters.* Journal of Alloys and Compounds, 2022. **909**: p. 164823.https://doi.org/10.1016/j.jallcom.2022.164823
30. Sabbah, H., *Numerical simulation of 30% efficient lead-free perovskite CsSnGeI3-based solar cells.* Materials, 2022. **15**(9): p. 3229.https://doi.org/10.3390/ma15093229
31. Peng, C.-H. and Y.-C. Lin, *SCAPS-1D Simulation of Various Hole Transport Layers' Impact on CsPbI2Br Perovskite Solar Cells Under Indoor Low-Light Conditions.* Solids, 2025. **6**(3): p. 31.https://doi.org/10.3390/solids6030031
32. Saha, S. and B. Chakraborty, *SCAPS-1D modeling and optimization of Rb2SnBr6-based lead-free perovskite solar cells.* Available at SSRN 5209294, 2025.https://ssrn.com/abstract=5209294
33. He, Y., et al., *Design and numerical investigation of a lead-free inorganic layered double perovskite Cs4CuSb2Cl12 nanocrystal solar cell by SCAPS-1D.* Nanomaterials, 2021. **11**(9): p. 2321.https://doi.org/10.3390/nano11092321
34. Kabir, I. and S. Mahmood, *Analysis of highly efficient perovskite solar cells with inorganic hole transport material.* Chinese Physics B, 2019. **28**(12): p. 128801.DOI 10.1088/1674-1056/ab520f
35. Hossain, M.K., et al., *An investigation of hole transport layers and electron transport layers to produce highly efficient K2TiI6-based perovskite solar cells.* Scientific Reports, 2025. **15**(1): p. 19014.https://doi.org/10.1038/s41598-025-98351-y
36. Abdelaziz, S., et al., *Investigating the performance of formamidinium tin-based perovskite solar cell by SCAPS device simulation.* Optical materials, 2020. **101**: p. 109738.https://doi.org/10.1016/j.optmat.2020.109738
37. Banik, S., et al., *Numerical simulation and performance optimization of a lead-free inorganic perovskite solar cell using SCAPS-1D.* Heliyon, 2024. **10**(1).https://doi.org/10.1016/j.heliyon.2024.e23985
38. Saif, A.e.A. and G. Alahmadi, *Optimization of HTL and ETL materials and parameters for high-efficiency CH 3 NH 3 SnI 3 perovskite solar cells.* AIMS Materials Science, 2025. **12**(5).https://doi.org/10.3934/matersci.2025046
39. Hossain, M.K., et al., *An extensive study on multiple ETL and HTL layers to design and simulation of high-performance lead-free CsSnCl3-based perovskite solar cells.* Scientific Reports, 2023. **13**(1): p. 2521.https://doi.org/10.1038/s41598-023-28506-2
40. Karmaker, H., A. Siddique, and B.K. Das, *Numerical investigation of lead free Cs2TiBr6 based perovskite solar cell with optimal selection of electron and hole transport layer through SCAPS-1D simulation.* Results in Optics, 2023. **13**: p. 100571.https://doi.org/10.1016/j.rio.2023.100571
41. Abdulmalik, M.O., et al., *Numerical study of 25.459% alloyed inorganic lead-free perovskite CsSnGeI3-based solar cell by device simulation.* East European Journal of Physics, 2022(4): p. 125-135.https://doi.org/10.26565/2312-4334-2022-4-12
42. Reza, M.S., et al., *A comprehensive investigation involving numerous HTL and ETL layers to design and simulate high-efficiency Ca3AsI3-based perovskite solar cells.* Inorganic Chemistry Communications, 2025. **172**: p. 113647.https://doi.org/10.1016/j.inoche.2024.113647
43. Alsalme, A., et al., *Optimization of photovoltaic performance of Pb-free perovskite solar cells via numerical simulation.* Molecules, 2022. **28**(1): p. 224.https://doi.org/10.3390/molecules28010224
44. Vulindlela, I., et al., *Design and computational investigation of PbS-based bifacial quantum dot-sensitized solar cells.* Results in Optics, 2025. **19**: p. 100818.https://doi.org/10.1016/j.rio.2025.100818